# Effects of Poloxamer 188 on Phospholipid Monolayer Morphology: An Atomic Force Microscopy Study

Guohui Wu and Ka Yee C. Lee*

*Department of Chemistry, the Institute for Biophysical Dynamics & the James Franck Institute, The University of Chicago, Chicago, Illinois 60637*

*Received September 4, 2008. Revised Manuscript Received November 6, 2008*

P188, a triblock copolymer of the form poly(ethylene oxide)−poly(propylene oxide)−poly(ethylene oxide) (PEO−PPO−PEO) is known as an effective membrane sealant. Using a dipalmitoylphosphatidylcholine monolayer at the air−water interface to mimic the outer leaflet of the cell membrane, we have examined the interaction between P188 and a phospholipid film. Atomic force microscopy (AFM) was used to investigate the morphological changes in the lipid monolayer induced by P188 insertion upon transferring the lipid/polymer film from the air−water interface onto a solid substrate. Our AFM results confirm that lipid packing regulates poloxamer insertion such that P188 only changes the morphology of a lipid monolayer when the lipid packing density is below that of the insertion threshold. By combining phase imaging and different driving forces in tapping mode AFM, our results further help reveal the distribution of poloxamers in the lipid monolayer with nanometer resolution.

## Introduction

Poloxamers or pluronics, a family of triblock copolymers with the structure of poly(ethylene oxide)−poly(propylene oxide)−poly-(ethylene oxide) (PEO−PPO−PEO), have recently attracted a great deal of attention as excellent membrane sealants with low toxicity.[1−5] When the membrane permeability increases dramatically in the case of trauma or diseases, the natural pathway for maintaining the normal permeability of cell membranes can be overwhelmed, rendering it incapable of arresting leakage in these permeabilized membranes. Under these circumstances, an alternative pathway is needed to help seal membranes to ensure the survival of the cells. It has been established that exogenous agents, such as poloxamer 188 and other members of poloxamers, can accomplish the task of membrane sealing rather well.[1] Poloxamer 188 (P188, MW = 8400 g/mol, with 80 wt % PEO content) was first shown to seal cells against loss of carboxyfluorescein dye after electroporation.[1,6−11] P188 has further been proven to be a successful sealing agent for various permeabilized cells, including skeletal muscle tissues after heat shock and intense irradiation,[12,13] red blood cells from sickle cell disease,[14] and neuronal cells after necrosis-inducing stimuli.[15] More recently, it has been demonstrated that P188 is an effective agent for treating cardiomyopathy and heart failure in muscular dystrophy.[2] Although it has been demonstrated that P188 is effective in restoring damaged cell membranes, the underlying mechanisms have only been investigated recently. Curiously, there have also been reports on other poloxamers, such as L61, which help in facilitating the transbilayer permeation of anticancer drug doxorubicin, rather than restoring membrane integrity. This facilitating effect has been found to be affected by the lipid composition.[16,17] Clearly, the membrane−poloxamer interaction calls for more detailed mechanistic studies.

A Langmuir lipid monolayer at the air−water interface serves as an effective model for the outer leaflet of the cell membrane. We and others have carried out studies at both the macroscopic and molecular levels on the interaction between poloxamers and lipid monolayers using Langmuir isotherms, insertion assays, and X-ray diffraction measurements.[18−22] Although fluorescence microscopy allows us to monitor the morphological changes in the lipid film upon the poloxamer's association, its resolution is limited to the micrometer length scale; the ability to directly visualize the mixed lipid/poloxamer system at a better resolution is highly desirable, as it can help reveal the distribution of poloxamers and lipids in biomembranes. Atomic force microscopy

* To whom correspondence should be addressed. Telephone: (773) 702-7068. Fax: (773) 702-0805. E-mail: kayeelee@uchicago.edu.

(1) Lee, R. C.; River, L. P.; Pan, F.-S.; Ji, L.; Wollmann, R. L. *Proc. Natl. Acad. Sci. U.S.A.* **1992**, *89*, 4524–8.
(2) Yasuda, S.; Townsend, D.; Michele, D. E.; Favre, E. G.; Day, S. M.; Metzger, J. M. *Nature* **2005**, *436*, 1025–1029.
(3) Greenebaum, B.; Blossfield, K.; Hannig, J.; Carrillo, C. S.; Beckett, M. A.; Weichselbaum, R. R.; Lee, R. C. *Burns* **2004**, *30*, 539–47.
(4) Wu, G.; Frey, S. L.; Maskarinec, S. A.; Lee, K. Y. C. *MRS Bull.* **2006**, *31*, 532–535.
(5) Kilinc, D.; Gallo, G.; Barbee, K. A. *Exp. Neurol.* **2008**, *212*, 422–430.
(6) Johnsson, M.; Silvander, M.; Karlsson, G.; Edwards, K. *Langmuir* **1999**, *15*, 6314–6325.
(7) Kostarelos, K.; Luckham, P. F.; Tadros, T. F. *J. Liposome Res.* **1995**, *5*, 117–130.
(8) Kostarelos, K.; Kipps, M.; Tadros, T. F.; Luckham, P. F. *Colloids Surf.* **1998**, *136*, 1–9.
(9) Kostarelos, K.; Luckham, P. F.; Tadros, T. F. *J. Chem. Soc., Faraday Trans.* **1998**, *94*, 2159–2168.
(10) Kostarelos, K.; Tadros, T. F.; Luckham, P. F. *Langmuir* **1999**, *15*, 369–376.
(11) Woodle, M. C.; Newman, M. S.; Martin, F. J. *Int. J. Pharm.* **1992**, *88*, 327–334.
(12) Padanilam, J. T.; Bischof, J. C.; Lee, R. C.; Cravalho, E. G.; Tompkins, R. G.; Yarmush, M. L.; Toner, M. *Ann. N. Y. Acad. Sci.* **1994**, *720*, 111–23.
(13) Hannig, J.; Zhang, D.; Canaday, D. J.; Beckett, M. A.; Astumian, R. D.; Weichselbaum, R.; Lee, R. C. *Radiat. Res.* **2000**, *154*, 171–177.
(14) Orringer, E. P.; Casella, J. F.; Ataga, K. I.; Koshy, M.; Adams-Graves, P.; Luchtman-Jones, L.; Wun, T.; Watanabe, M.; Shafer, F.; Kutlar, A.; Abboud, M.; Steinberg, M.; Adler, B.; Swerdlow, P.; Terregino, C.; Saccente, S.; Files, B.; Ballas, S.; Brown, R.; Wojtowicz-Praga, S.; Grindel, J. M. *JAMA, J. Am. Med. Assoc.* **2001**, *286*, 2099–106.
(15) Marks, J. D.; Pan, C.-y.; Bushnell, T.; Cromie, W.; Lee, R. C. *FASEB J.* **2001**, *15*, 1107–1109.
(16) Zhirnov, A. E.; Demina, T. V.; Krylova, O. O.; Grozdova, I. D.; Melik-Nubarov, N. S. *Biochim. Biophys. Acta* **2005**, *1720*, 73–83.
(17) Krylova, O. O.; Melik-Nubarov, N. S.; Badun, G. A.; Ksenofontov, A. L.; Menger, F. M.; Yaroslavov, A. A. *Chem.−Eur. J.* **2003**, *9*, 3930–3936.
(18) Weingarten, C.; Santos Magalhaes, N. S.; Baszkin, A.; Benita, S.; Seiller, M. *Int. J. Pharm.* **1991**, *75*, 171–9.
(19) Maskarinec, S. A.; Hannig, J.; Lee, R. C.; Lee, K. Y. C. *Biophys. J.* **2002**, *82*, 1453–1459.
(20) Maskarinec, S. A.; Lee, K. Y. C. *Langmuir* **2003**, *19*, 1809–1815.
(21) Wu, G.; Majewski, J.; Ege, C.; Kjaer, K.; Weygand, M. J.; Lee, K. Y. C. *Phys. Rev. Lett.* **2004**, *93*, 028101-4.
(22) Wu, G.; Majewski, J.; Ege, C.; Kjaer, K.; Weygand, M. J.; Lee, K. Y. C. *Biophys. J.* **2005**, *89*, 3159–3173.

10.1021/la802908x CCC: $40.75 
Published on Web 01/13/2009

(AFM)[23] is an excellent, nondestructive, high-resolution technique for investigating adsorbed film structures. Height and phase mode AFM images depend heavily on the nanomechanical properties of the film,[24] which can be probed by an AFM tip with varying free driving-amplitudes $A_0$ and the set-point ratios $r_{sp}$ in tapping mode. When the tip is brought close to the sample surface, the tip interacts with the sample as well as the contamination layer on the surface, thereby changing the vibrational characteristics of the cantilever, such as the resonance frequency, phase angle, and amplitude.[25] For a heterogeneous surface, this property is important in using AFM for mapping out different components in composite materials and differentiating regions of varying surface adhesion or hardness. In this work, we use height imaging AFM to monitor morphological changes in lipid films induced by poloxamers. Moreover, by applying phase imaging and different driving forces in tapping mode AFM (TMAFM) to probe surface heterogeneity, we have also determined the distribution of lipids and poloxamers in the film with nanometer resolution.

## Materials and Methods

**Materials.** 1,2-Dipalmitoyl-*sn*-glycero-3-phosphocholine (DPPC) was purchased in powder form from Avanti Polar Lipids (Alabaster, AL) and used without further purification. The DPPC monolayer was spread from a chloroform solution at a concentration of 0.5 mg/mL. DPPC was chosen as the model lipid system for this study, as it allows us to directly compare the results obtained here via AFM with earlier work on the same system using monolayer insertion assay, fluorescence microscopy, and X-ray scattering techniques. Furthermore, DPPC exhibits phase coexistence under the experimental conditions and thus allows for clear identification of the effects of poloxamers on lipid organization.

Throughout the experiments, pure water (resistivity $\geq 18\ M\Omega \cdot cm$) obtained from a Milli-Q UV Plus system (Millipore, Bedford, MA) was used. A stock solution of 200 mg/mL P188 was prepared by dissolving poloxamer (BASF, Parisippany, NJ) in pure water. High-grade mica (Ted Pella Inc., Redding, CA) was used as a substrate to support the transferred lipid monolayer for AFM imaging.

**Preparation of Thin Films at the Air−Water Interface.** To test whether P188 selectively interacts with damaged membranes, the step-down protocol described previously[19] was adopted to prepare lipid monolayers and lipid/P188 thin films at the air−water interface. Briefly, a DPPC monolayer was spread on a home-built Teflon Langmuir trough and compressed to 30 mN/m (the bilayer equivalent pressure[26,27]) to mimic the intact packing of a membrane and held constant while P188 was injected into the subphase to achieve the final concentration of 50 mM. The change of surface area was monitored for 10 min for any insertion of P188 into monolayer at a constant pressure. If no insertion occurred, then the surface pressure was lowered by 2 mN/m and was again held constant for 10 min in each step, until P188 insertion occurred as indicated by the expansion of the barriers. Such an expansion was needed to release the packing stress in order to keep the pressure constant.

The surface pressure−area ($\pi - A$) isotherm of the step-down experiment is shown in Figure 1; the isotherm is in agreement with previous results obtained in our laboratory.[19] Before and after P188 insertion into the monolayer, the films were transferred from the air−water interface onto a freshly cleaved mica substrate and imaged with AFM. Deposition conditions used in our experiments are denoted by arrows in Figure 1.

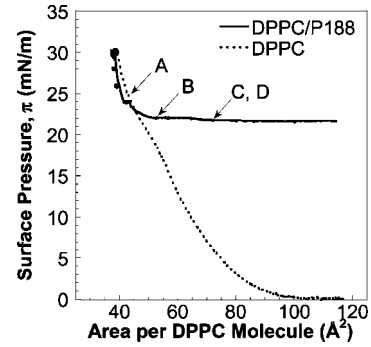


**Figure 1.** "Step-down" isotherms of DPPC monolayer with P188 in the water subphase at 30 °C. Monolayer films were compressed to 30 mN/m, and then P188 was injected into the subphase. Afterward, the surface pressure was lowered by 2 mN/m and held constant for 10 min in each step, until a large change in the area per lipid molecule was observed, resulting in the expansion of the barriers. The arrows point to conditions under which the film was transferred from the air−water interface onto a solid substrate for imaging with AFM.

Pure P188 film at the air−water interface was also prepared by injecting P188 into the water subphase without any lipid spread at the water surface. The P188 film was then deposited onto a solid substrate using the protocol described below.

**Film Transfer from the Air−Water Interface onto a Solid Substrate.** To image a monolayer with AFM, it is necessary to transfer the monolayer from the air−water interface to a solid substrate before the spreading of the lipid monolayer mica was mounted on a magnetic stainless steel disk and positioned at the bottom of the Langmuir trough in the subphase, with its freshly cleaved surface underneath and parallel to the air−water interface. The inverted Langmuir−Schaeffer method, whereby the water level was slowly lowered until the mica surface was exposed to air, was used for the transfer after the monolayer was compressed to the desired surface pressure.[28] A constant surface area was maintained during the transfer process. This procedure yields a supported monolayer in which the polar groups are in contact with the mica surface and the hydrophobic portion is exposed to the air. Careful control of deposition speed is essential to avoid artifacts. The deposition process was monitored by fluorescence microscopy (FM) to ensure that no change larger than the resolution of FM (micrometer scale) occurred to the monolayer morphology during the transfer process.[29] The supported monolayer was then dried overnight at room temperature in a covered container.

**AFM Imaging.** A MultiModeNanoscope IIIA atomic force microscope (model MMAFM-2, Veeco Instruments, Santa Barbara, CA) was used for AFM imaging. Tapping mode imaging was performed using a type J scanner (maximum scan size 125 $\mu$m) and Olympus TappingMode Etched silicon probes (Veeco Instruments), with a typical radius of less than 10 nm and a nominal spring constant of 42 N/m. The drive frequency was 270−300 kHz. A drive amplitude between 8 and 80 mV, corresponding to an amplitude of the freely oscillating cantilever $A_0$ (when the tip is far away from the surface) of 10−112 nm, was tested. During a scan, the amplitude of the cantilever oscillation was maintained at a set-point amplitude, $A_{sp}$, by adjusting the vertical sample position. The set-point ratio, $r_{sp} = A_{sp}/A_0$, is varied from 0.52 to 0.81 of the free amplitude in our experiments. The images were recorded both in height and phase modes with a frame rate of 512 × 512.

## Results and Discussion

To monitor morphological changes of a DPPC monolayer induced by P188 insertion, AFM images were taken for both pure DPPC and DPPC/P188 systems. The "step-down" isotherm

(23) Shao, Z.; Mou, J.; Czajkowksy, D. M.; Yang, J.; Yuan, J. Y. *Adv. Phys.* **1996**, *45*, 1–86.
(24) Garcia-Manyes, S.; Domenech, O.; Sanz, F.; Montero, M. T.; Hernandez-Borrell, J. *Biochim. Biophys. Acta* **2007**, *1768*, 1190–1198.
(25) Magonov, S. N.; Elings, V.; Whangbo, M. H. *Surf. Sci.* **1997**, *375*, L385−L391.
(26) Marsh, D. *Biochim. Biophys. Acta* **1996**, *1286*, 183–223.
(27) Shaikh, S. R.; Dumaual, A. C.; Jenski, L. J.; Stillwell, W. *Biochim. Biophys. Acta* **2001**, *1512*, 317–328.
(28) Ege, C. *Templating effect of lipid membranes on Alzheimer's amyloid beta peptide by X-ray scattering*; University of Chicago: Chicago, 2004.
(29) Lee, K. Y. C.; Lipp, M. M.; Takamoto, D. Y.; Ter-Ovanesyan, E.; Zasadzinski, J. A.; Waring, A. J. *Langmuir* **1998**, *14*, 2567–2572.

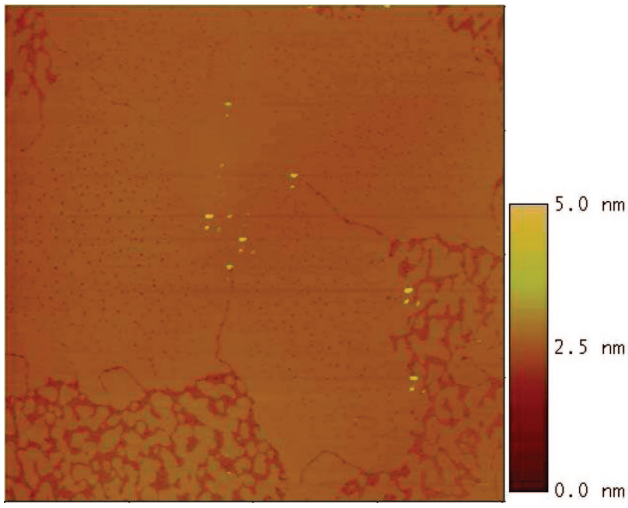


**Figure 2.** AFM height image (10 $\mu$m × 10 $\mu$m) of a DPPC monolayer deposited on a mica substrate from the air/water interface at $\pi$ = 24 mN/m ($A_{DPPC}$ = 53 Å$^2$).

results show that P188 only started to insert into a DPPC monolayer at surface pressures $\pi$ below 24 mN/m, and a surface pressure of 22 mN/m was maintained during subsequent insertions (Figure 1). The DPPC/P188 monolayer was therefore transferred and imaged with AFM at 24 and 22 mN/m, corresponding to the absence and the presence of P188 in the DPPC monolayer, respectively. The detailed conditions of preparing the transferred films are marked in Figure 1.

**Surface Morphology.** *Pure DPPC Monolayer.* Figure 2 shows the AFM image of pure DPPC at 24 mN/m. At 24 mN/m, the isotherm indicates that the DPPC monolayer exists at the end of the liquid-expanded/condensed phase transition with an average area per molecule of $A_{DPPC}$ = 53Å$^2$. The corresponding AFM image (Figure 2) is characterized by ~15 $\mu$m condensed domains, as shown by the large flower-shaped area with smooth surface in bright color. The condensed phase, with hydrocarbon chains in the trans-conformation and tilting at a small angle relative to the surface normal, is brighter in the AFM image, as the brighter color reflects a greater surface height. The observed height difference is 0.5 ± 0.2 nm, owing to the difference in height between the condensed phase and the fluid phase in the lipid film.[30]

*DPPC Monolayer with P188 in the Subphase.* Figure 3 shows AFM height images of films transferred from the air−water interface onto mica substrates with P188 present in the subphase. At 24 mN/m, the "step-down" isotherm indicates that P188 is not incorporated in the DPPC monolayer, and Figure 3A indeed shows morphological features similar to those for pure DPPC monolayers (Figure 2).

It is worth noting that pure P188 does not show any preferred adhesion onto the mica surface in water as shown in our control experiments (data not shown). In these control experiments, a drop of P188 solutions with a concentration up to 20 mg/mL was deposited on freshly cleaved mica and incubated for ~30 min in an enclosed container to minimize water evaporation. Imaging of the mica surface was then performed in fluid using TMAFM with a minimum force and revealed a surface morphology identical to that of a bare mica surface, indicating no P188 adsorption on mica. Therefore, almost no free P188 chains inside the subphase should be trapped between the DPPC monolayer and the mica surface during the deposition process, and only the film at the air−water interface was being transferred onto the mica surface.

Under conditions B ($\pi$ = 22 mN/m and $A_{DPPC}$ = 62 Å$^2$) and C ($\pi$ = 22 mN/m and $A_{DPPC}$ = 77 Å$^2$) indicated in Figure 1, the nominal lipid packing decreased and P188 was incorporated into DPPC monolayers, leading to dramatic changes in the corresponding morphology of DPPC/P188 films as shown in Figure 3B and C. The morphology of the DPPC/P188 film in Figure 3B still maintains some features of pure DPPC as the ~10 $\mu$m condensed domain remains discernible. However, some regions in Figure 3B appear as highly curled spirals (or paisley pattern) possibly due to the chirality of the DPPC molecule itself.[31]

It is obvious from Figure 3 that the incorporation of P188 in the lipid film has a distinct effect on film morphology. The distinct network like structure comes from the opposite driving forces for macro-phase separation and mixing, as predicted by Zhang, et al.[32] While the hydrophobic mismatch between the acyl chain region of the lipid and the PPO portion of the polymer would lead to macrophase separation between DPPC and P188,[32,33] the long-range soft repulsive interaction between the hydrophilic blocks of P188 would favor complete mixing between the two species. The optimal network structure is therefore a balance between these opposing forces. The enhanced ruggedness of the domain edge results from the modification of the line tension by the presence of the polymer. It has long been established that the equilibrium domain morphology is determined by the balance between line tension and electrostatic repulsion between lipids.[34,35] Breakup of smooth micrometer-size domains into nanometer-scale features reflects a decrease in line tension. Such a change in line tension likely also plays a role in inducing the intricate "paisley" pattern shown in Figure 3B, which appears to exhibit a uniform width of the curved stripes. However, further studies are needed for a more thorough understanding of these pattern formations in this lipid/P188 system.

The lipid packing density in the monolayer decreased further from condition B to that of C and D, and thus causing further P188 insertion. As it is obvious from Figure 3C and D, the morphology deviates a great deal from that of pure DPPC (Figures 2 and 3A). It should be noted that both C and D in Figure 3 were obtained from different parts of the same film under otherwise identical conditions. Our previous work has suggested that, at large nominal areas per lipid, the DPPC/P188 film is heterogeneous and consists of either lipid-rich or poloxamer-rich patches with a length scale as large as 15 mm as revealed by fluorescence microscopy.[22] Here, our AFM images corroborate this heterogeneous surface phenomenon.

A close examination of the atomic force micrograph reveals three different height levels in Figure 3C. By comparing AFM images of the DPPC/P188 film and pure DPPC monolayer images all with the same $z$ range, the dark (e.g.,"a" in Figure 3C) and intermediate brightness portions (e.g., "b" in Figure 3C) can be attributed to the disordered and condensed phases of the lipid monolayer, respectively, which have a height difference in the range of 0.5 ± 0.2 nm. The portion of the film with the highest level of brightness (e.g., "c" in Figure 3C) is found to be ~3 nm higher than the part in the intermediate brightness range, making it about 5 nm in overall height when one takes into account the lipid monolayer thickness of ~2 nm. The only constituent that

(30) Nielsen, L. K.; Vishnyakov, A.; Jorgensen, K.; Bjornholm, T.; Mouritsen, O. G. *J. Phys.: Condens. Matter* **2000**, *12*, A309−A314.
(31) Selinger, J. V.; Wang, Z. G.; Bruinsma, R. F. *Mater. Res. Soc. Symp. Proc.* **1993**, *292*, 235–240.
(32) Zhang, D.; Carignano, M. A.; Szleifer, I. *Phys. Rev. Lett.* **2006**, *96*, 028701/1−028701/4.
(33) Frey, S. L.; Zhang, D.; Carignano, M. A.; Szleifer, I.; Lee, K. Y. C. *J. Chem. Phys.* **2007**, *127*, 114904/1–114904/12.
(34) McConnell, H. M.; Moy, V. T. *J. Phys. Chem.* **1988**, *92*, 4520–5.
(35) McConnell, H. M. *Annu. Rev. Phys. Chem.* **1991**, *42*, 171–95.

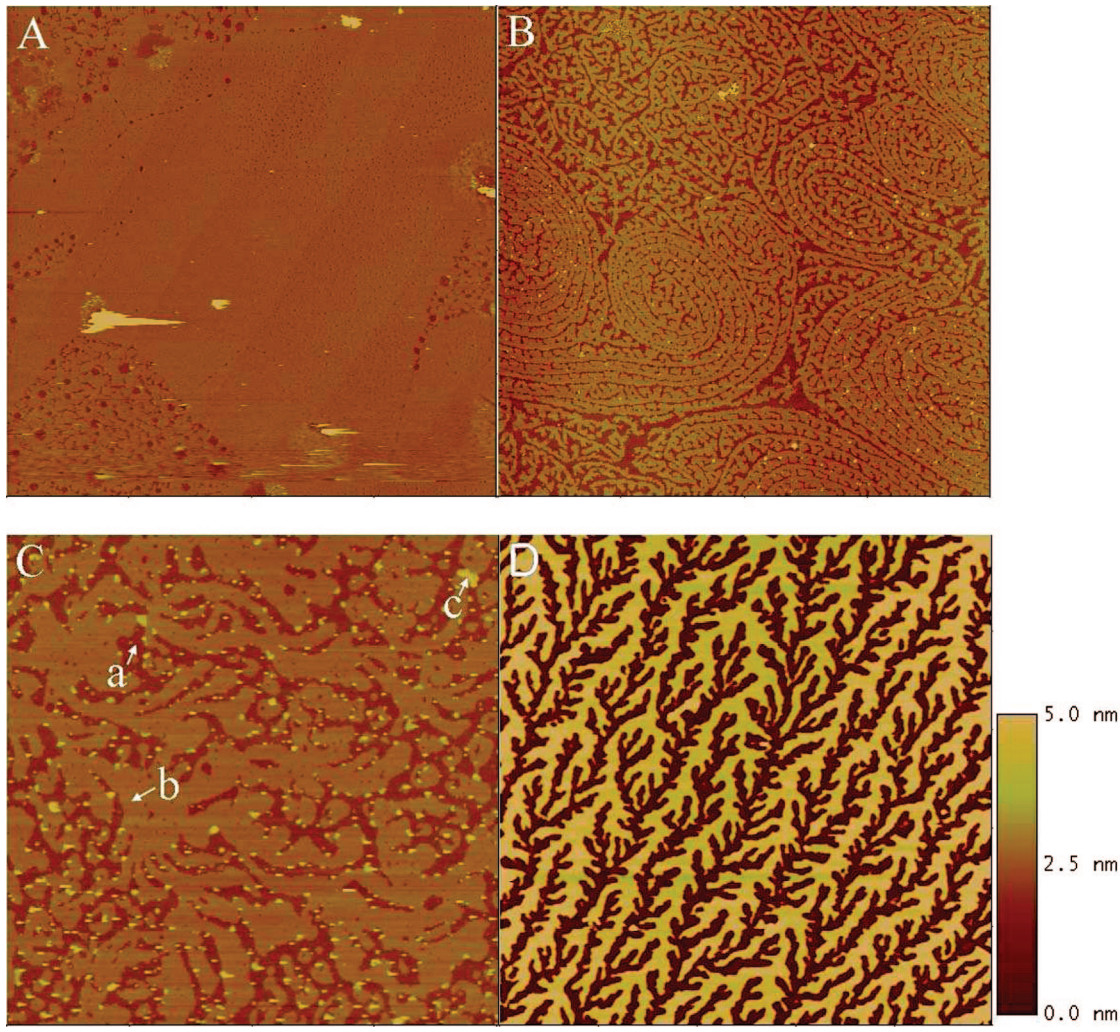


**Figure 3.** AFM height images (10 $\mu$m × 10 $\mu$m) of a DPPC monolayer with P188 in the subphase deposited from the air−water interface onto a mica substrate; the imaging was performed in air. The film was transferred at (A) $\pi$ = 24 mN/m ($A_{DPPC}$ = 53 Å$^2$); (B) $\pi$ = 22.1 mN/m ($A_{DPPC}$ = 62 Å$^2$); and (C, D) $\pi$ = 21.8 mN/m ($A_{DPPC}$ = 82 Å$^2$). (A), (B), and (C, D) correspond to the film at the air/water interface under conditions as indicated by the arrows in Figure 1. The images confirm that P188 is incorporated into the DPPC monolayer in (B) and (C, D) but not in (A). Images (C) and (D) were transferred from different parts of the same film under otherwise identical conditions; they confirm the surface heterogeneity of the DPPC/P188 film as previously shown by X-ray measurements,[22] with (C) being a relatively lipid-rich region and (D) a P188-rich region. Arrows in (C) point to three representative height levels.

can give rise to such a height in the transferred film is the P188 residing in the film (a pure P188 film on mica has a thickness in the 5−7 nm range as shown in the next section). Figure 3D shows a surface height that varies between 0.7 and 6 nm above bare mica but with most of the area exhibiting a height of ∼6 nm, which indicates that P188 is the dominant component in the region imaged. Although from the same transferred film, Figure 3C and D shows distinctly different morphologies. Our observations are therefore in line with the assignment of Figure 3C and D representing the relatively DPPC-rich region and the P188-rich region in the DPPC/P188 system, respectively.

Our previous X-ray diffraction data show that DPPC in the absence and presence of P188 exhibits identical unit cell and molecular tilt at the same surface pressure, suggesting that P188 is separated from the ordered DPPC phase and does not affect the molecular packing.[22] Therefore, the surface area fraction occupied by P188 can be estimated as $(A_{DPPC/P188}-A_{DPPC})/A_{DPPC/P188}$ by comparing the isotherm of a pure DPPC monolayer with that of a DPPC/P188 monolayer. From the isotherm of a pure DPPC monolayer, the area per DPPC molecule at 22 mN/m reads $A_{DPPC}$ = 57 Å$^2$. With this value, the average surface occupancy of P188 in the film of DPPC/P188 is estimated to be 8% under condition B (Figure 1), and 30% under conditions C and D (Figure 1). As revealed by X-ray diffraction, the insertion of P188 induces surface heterogeneity and gives rise to relatively lipid-rich and lipid-poor regions in the same film;[21,22] therefore, the exact content of P188 in the region being imaged in the transferred DPPC/P188 film can actually vary from one location to another.

*P188 Film.* At the air−water interface, at 30 min after injection the surface pressure of the P188 film reached 25 mN/m without barrier compression, indicating that P188 is highly surface active. AFM images of a transferred pure P188 film are shown in Figure 4. Figure 4A displays a morphology often seen in nonequilibrium crystallization of polymer thin films.[36] With the elimination of solvent after the drying process, the transferred P188 film exhibits a seaweed pattern. The seaweed pattern is characterized by broad growing tips that split intermittently; such splitting normally results in the dominance of one of the newly formed branches over the others. Repeating this process leads to a cascade of branching events.[36] The measured thickness of

(36) Ferreiro, V.; Douglas, J. F.; Warren, J. A.; Karim, A. *Phys. Rev. E* **1992**, *65*, 042802-4.

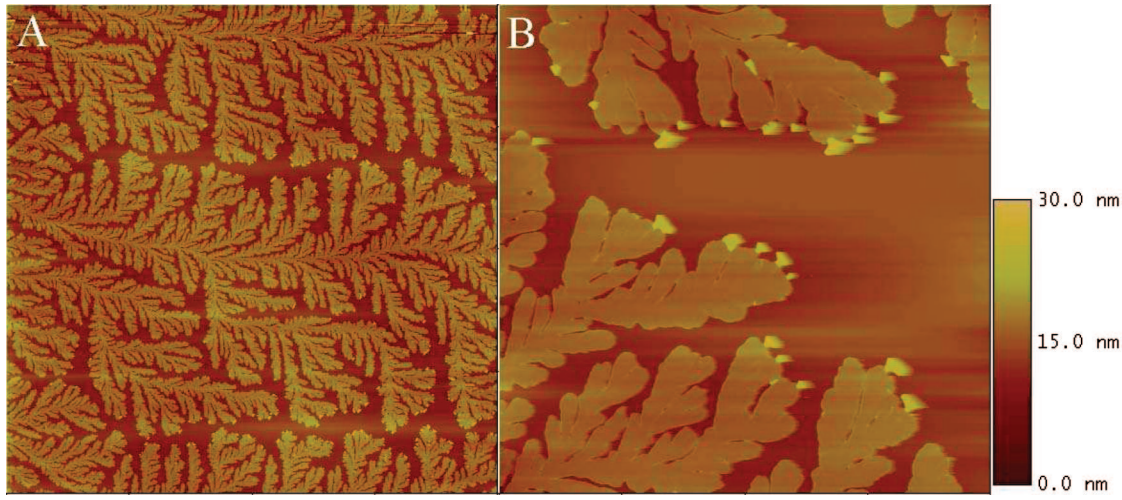


**Figure 4.** AFM height images of a pure P188 film transformed from the air−water interface onto a mica substrate. (A) 80 $\mu$m × 80 $\mu$m; (B) 10 $\mu$m × 10 $\mu$m. (B) is a zoomed-in image of (A).

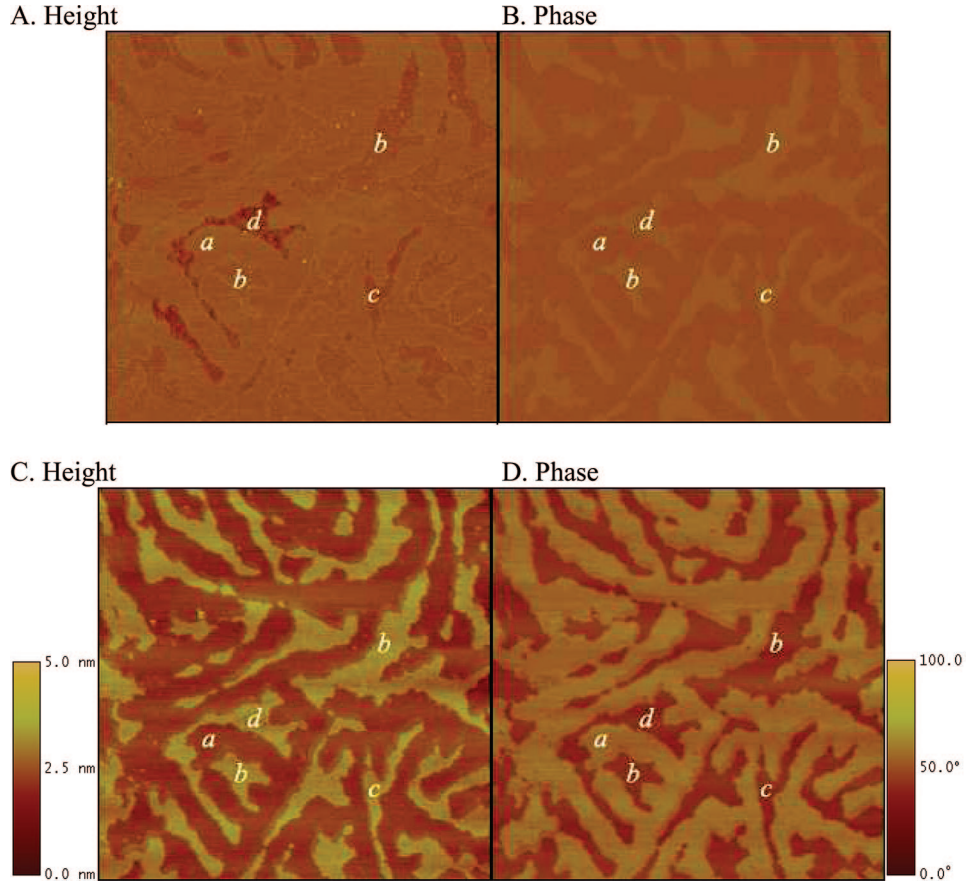


**Figure 5.** AFM images for a DPPC/P188 film transferred at $\pi$ = 22 mN/m, $A_{DPPC}$ = 62 Å$^2$) from the air−water interface onto a mica substrate and imaged in air: (A, B) light tapping, $A_{sp}$ = 14 nm, $A_0$ = 18 nm, $r_{sp}$ = 0.78; (C, D) hard tapping, $A_{sp}$ = 40 nm, $A_0$ = 53 nm, $r_{sp}$ = 0.75. Both height (A, C) and phase (B, D) images are 2 $\mu$m × 2 $\mu$m.

the P188 film is 5−7 nm; this thickness is similar to the highest portion of the film in Figure 3C and D. Furthermore, the lipid/P188 films in Figure 3C and D also share some similar features of the seaweed pattern in Figure 4, such as broad tips and split branches. These observations evidence the presence of a large amount of P188 in the DPPC monolayer (especially in the case of Figure 3D), resulting in a film morphology quite different from that of pure DPPC.

**Surface Heterogeneity.** To gain further insight into the lipid organization and polymer distribution, TMAFM was performed on the DPPC/P188 film on a mica support under condition B in Figure 1. Tapping mode was conducted by varying $r_{sp}$ and $A_0$. The height and phase images are shown in Figure 5 recorded at two $A_0$ values of 18 and 53 nm, with corresponding $r_{sp}$ values of 0.78 and 0.75, respectively. The effective force between the AFM tip and the sample surface increases with decreasing $r_{sp}$

and increasing $A_0$; we shall henceforth refer to tapping conditions in Figure 5A and B ($A_0 = 18$ nm and $r_{sp} = 0.78$) as light tapping and those in Figure 5C and D ($A_0 = 53$ nm and $r_{sp} = 0.75$) as hard tapping.

*Light Tapping.* For light tapping, the height image shows several height levels as indicated by, for example, regions marked as "a", "b", "c", and "d" in Figure 5A. The height detected for "a" is similar to that for "b", and both are higher than region "c" by ~0.4 nm; both "a" and "b" are higher than region "d" by ~0.8 nm. Meanwhile, region "a" has a smooth surface, with a measured roughness of <0.1 nm, while region "b" is slightly rougher (roughness ~ 0.14 nm), and region "d" is the roughest (roughness ~ 0.2 nm).

While the height mode shows three distinct height levels, the phase image obtained for light tapping shows only two levels with a phase shift of ~4°. As the phase mode AFM is sensitive to surface properties such as composition and viscoelasticity, the contrast here suggests that there are two kinds of materials adsorbed to the substrate. The material in "a" differs from that in regions "b", "c", and "d", with the latter three regions appearing to have the same surface properties. Previous characterization of mixed DPPC/P188 monolayers at the air−water interface with X-ray scattering techniques[21,22] has revealed the following two observations: (1) There exists phase separation between the lipid and the poloxamer at the surface, with one phase as ordered 2-D crystallites composed of pure DPPC and the other as a disordered polymer-rich phase; (2) P188, being completely excluded from DPPC crystallites, has to stay in the disordered region of the mixed film. Therefore, the two different materials as shown in the phase images should correspond to (I) the DPPC condensed phase and (II) the disordered DPPC/P188 phase.

Since a condensed DPPC domain should have a rather uniform thickness, it is unlikely for the bright color (larger phase shift) regions in Figure 5B with height variations up to ~ 0.8 nm (Figure 5A) to be from the condensed lipid phase. The only reasonable assignment is that region "a" corresponds to the condensed DPPC phase (I) while regions "b", "c" and "d" are populated by the disordered DPPC/P188 phase (II).

*Hard Tapping.* The height image is dramatically altered under hard tapping (Figure 5C), and the phase images show a contrast inversion (Figure 5D). The height image reveals only two height steps with a difference of ~0.9 nm. The presence of only two height steps agrees well with the existence of two surface components as indicated in the phase images. Interestingly, region "b" is now found to be higher than region "a", though no height difference between them is revealed under light tapping. The contrast between regions "a" and "d" is also reversed compared to that with light tapping. The height image under hard tapping conditions thus reflects a height difference between coexisting phases in a manner opposite to the topography under light tapping; this has been previously reported for the self-assembled monolayer of alkanethiols on gold, where the alkanethiol-covered region appears lower compared to the surrounding Au background.[37] Similar contrast reversion was also reported for the surfactin/DPPC film.[38]

Such a height reversal phenomenon can be explained by the difference in the interaction of the AFM probe with the two surface components. In TMAFM, a surface region of larger amplitude damping is recorded as higher in topography and hence brighter in the height image. Height image contrast is influenced not only by the height variation on the surface but also by the amount of amplitude damping. The maximum kinetic energy available for the freely oscillating cantilever is $W = {}^1/_2 k A_0^2$ at each oscillation,[39] with $k$ as the force constant of the free cantilever. When the oscillating tip approaches the surface, the maximum kinetic energy increases if there is an attractive tip−sample interaction to provide an additional energy but decreases when a repulsive tip−sample interaction is present. Therefore, to maintain a certain $A_{sp}$, the damping of the amplitude is enhanced when the tip−sample interaction is attractive[37] and such a higher degree of damping manifests itself as increased sample height.

Our suggested identification of surface components (I) and (II) agrees with this explanation. The DPPC/P188 samples have two surface regions of different hydrophilicity. In the condensed DPPC phase (I) (identified as region "a"), the hydrocarbon tail is strongly hydrophobic; in the disordered phase (II) with the mixture DPPC/P188 (identified as regions "b", "c", and "d"), it is relatively less hydrophobic due to the presence of P188. On the other hand, the tip of the Si cantilever is covered with $SiO_2$ and is strongly hydrophilic. Hence, the interaction between the tip and DPPC/P188 region ((II); "b", "c", and "d" as indicated in Figure 5C) is relatively attractive, while the interaction between the tip and the DPPC hydrocarbon region ((I); "a" in Figure 5C) is relatively repulsive.

For light tapping, the tip−sample interaction is negligible and is affected by the surface contamination layer. When the tapping amplitude is increased, the cantilever is more significantly affected by the strong attractive interactions in the disordered DPPC/P188 region than those in the condensed DPPC region. The damping of the amplitude increases with attractive tip−sample interactions and is significantly larger on the disordered DPPC/P188 region, rendering the regions "b", "c", and "d" brighter in the height image in Figure 5C.

The reverse in contrast in the height images at light and hard tapping emphasizes the necessity of performing AFM experiments and interpreting the data in a careful and systematic manner. A rule of thumb is the application of a minimum force on the sample surface, as this not only prevents irreversible sample damages but also reduces the effects of sample−probe interactions, which can transiently or otherwise deform the surface topography and give rise to erroneous sample heights.

Furthermore, different components have different surface stiffness and therefore varying elastic deformations associated with the tip−sample interaction. A softer material leads to a larger contact area with the AFM tip, and the duration of tip−sample contact is longer on a soft material than on a hard one. These effects are further enhanced at large $A_0$ and small $r_{sp}$. Consequently, the phase shift is greater on a softer material than on a harder one.[25,40] This shows that the hydrocarbon tails of the condensed DPPC region ("a": the phase shifted by 12° when the tapping was changed from light to hard) are softer compared to the disordered DPPC/P188 regions ("b", "c", and "d": the phase shifted by −12° from light to hard tapping), which is reasonable, as the hydrocarbon tails are "oil"-like while P188 is dried and in the crystallized form, which in turns stiffens the surface.

## Conclusion

AFM has been used to study changes in lipid monolayer morphology induced by the incorporation of poloxamers. Height imaging results confirm that the lipid density regulates the insertion of poloxamers into the lipid monolayer: Above the

(37) Whangbo, M. H.; Bar, G.; Brandsch, R. *Appl. Phys. A: Mater. Sci. Process.* **1998**, *66*, S1267−S1270.
(38) Deleu, M.; Nott, K.; Brasseur, R.; Jacques, P.; Thonart, P.; Dufrene, Y. F. *Biochim. Biophys. Acta* **2001**, *1513*, 55–62.
(39) Rao, S. S. *Mechanical Vibrations*, 3rd ed.; Addison-Wesley: New York, 1995; p 600.
(40) Pethica, J. B.; Oliver, W. C. *Phys. Scr.* **1987**, *T19A*, 61–66.

"insertion" surface pressure, there is no poloxamer incorporation into the lipid film and hence the film morphology remains unaltered from the pure DPPC monolayer; below the "insertion" pressure, the morphology deviates further from that of the lipid monolayer with decreasing nominal lipid density, until eventually the morphology shows many common features with those of pure poloxamers.

Phase imaging is a powerful extension of TMAFM height imaging, as it provides nanometer scale information on surface properties of the system in addition to the simple topographical mapping described. Phase imaging results unambiguously confirm the existence of two species on the surface. In addition, height images of DPPC/P188 films further show drastically different contrasts between light tapping and hard tapping. These differences help reveal the surface distribution of lipids and poloxamers. In the future, a more direct way to identify the surface species can be achieved by chemical force microscopy,[41] where the tip can be functionalized by a material with the desired chemistry to better identify the chemical nature of the different regions observed by AFM. Besides, time-of-flight secondary ion mass spectrometry can also be used to identify chemical heterogeneity.[42] Unlike the above-mentioned alternatives, this current study provides a high resolution mapping of compositional distributions without the need for complicated functionalization or special instrumentation.

The localization of P188 in the lipid matrix confirms that P188 intercalates into the lipid monolayer with a packing density below that of the insertion threshold. The presence of poloxamers may induce the expansion of the membrane and hence the closure of defects ("pores") in the structurally compromised membranes resulting from trauma or diseases. Our AFM data presented here provide direct visualization of lipid/poloxamer films with nanometer resolution, revealing morphological changes that give rise to intricate patterns when P188 is present. Theoretical elucidation of the mechanisms for these pattern formations may lead to a better understanding of the underlying physical forces involved. Future work should explore the effects of poloxamers on membrane models involving unsaturated lipids and cholesterol to provide a more representative model of mammalian cell membranes.

**Acknowledgment.** This work was supported in part by the University of Chicago MRSEC program of the NSF (DMR-0213745). G.W. acknowledges the support of Burroughs Wellcome Fund Interfaces No. 1001774.

LA802908X

(41) Noy, A.; Vezenov, D. V.; Lieber, C. M. *Annu. Rev. Mater. Sci.* **1997**, *27*, 381–421.

(42) McQuaw, C. M.; Sostarecz, A. G.; Zheng, L.; Ewing, A. G.; Winograd, N. *Langmuir* **2005**, *21*, 807–813.